Composite Structures 143 (2016) 336–346

Contents lists available at ScienceDirect

Composite Structures

journal homepage: www.elsevier.com/locate/compstruct

Geometrical nonlinear free vibration analysis of FG-CNT reinforced composite flat panel under uniform thermal field

Kulmani Mehar, Subrata Kumar Panda *

Department of Mechanical Engineering, National Institute of Technology Rourkela, 769008, India

ARTICLE INFO

Article history:
Available online 22 February 2016

Keywords:
Nonlinear vibration
FEM
FG-CNT
HSDT
Green-Lagrange nonlinearity
Micromechanical model

ABSTRACT

The nonlinear free vibration behavior of functionally graded carbon nanotube reinforced composite flat panel is investigated using temperature dependent material properties for different grading. The carbon nanotube reinforced composite flat panel model has been developed mathematically using the higher-order shear deformation theory and Green-Lagrange nonlinearity. The present mathematical model has included all the nonlinear higher-order terms for the sake of generality. Further, the responses are computed numerically using the direct iteration method in conjunction with the finite element method. The validity and the convergence behavior of the present nonlinear model have been checked and the effect of different design parameters on the nonlinear vibration responses are discussed in detail.

1. Introduction

Carbon nanotube (CNT) was discovered by Iijima [1] when he was working in the laboratory to determine the crystal structure of the nanotubes synthesized from carbon molecules. It is a special arrangement of carbon atoms in cylindrical form, and it possess excellent mechanical, thermal, electrical and chemical properties as compared to other available conventional and advanced materials. Due to its high strength, thermal stability and corrosion resistance, CNT finds its applications in the industries like aerospace, nuclear plant and marine structures [2]. In order to achieve the desired strength in high-performance engineering structure, the functionally graded carbon nanotube reinforced composites (FG-CNTRCs) are regarded as the substitute for the available functional materials. It is also a fact that a small amount of the CNT (2–5%) can also improve a considerable value of the stiffness and strength of the composite material [3,4].

Researchers have already devised various methods and formulation for the evaluation of the effective material properties of CNT and/or CNT reinforced composites namely, molecular dynamic (MD) simulation [5–7], representative volume element (RVE) method [8,9], extended rule of mixture [10,11] and Mori–Tanaka scheme [12,13] and so on. Further the structural responses such as vibration, bending and buckling behavior are computed using the available numerical and analytical or 3D elasticity method. In this regard, some of the significant contributions are discussed herewith to make the article self-explanatory. The FG-CNTRC plate is graded in the thickness direction [14,15] and/or longitudinal directions [16] to achieve the tailor-made properties. Rokni et al. [17] investigated the free vibration behavior of axially functionally graded multi-wall carbon nanotube (MWCNT) reinforced polymer composite beams using the modified couple stress theory. The stability behavior of the single-wall carbon nanotube (SWCNT) beam using Timoshenko beam theory (TBT) in conjunction with nonlocal elasticity investigated by Murmu and Pradhan [18]. Formica et al. [19] were computed the free vibration responses of the CNTRC, and the effective material properties are evaluated using Mori–Tanaka scheme.

The nonlinear responses (vibration, bending and buckling) of the composite structure are analyzed using different nonlinear kinematics (von-Karman and Green-Lagrange) in the framework of the available shear deformation and classical theories. The thermal buckling and the post-buckling responses of the FG-CNTRC flat panel analyzed by Shen and Zhang [20] using TBT and von-Karman geometric nonlinearity. Shen and Xiang [21] further investigated the nonlinear bending, vibration and post-buckling behavior of the FG-CNTRC beam resting on elastic foundations using the higher-order shear deformation theory (HSDT). Shiau and Kuo [22] investigated the thermal buckling behavior of the sandwich panel using first-order shear deformation theory (FSDT). Zhu et al. [23] used FSDT model for investigating the free vibration and the bending behavior of the FG-CNTRC plate. Shen [24] investigated the thermal post-buckling behavior of the CNTRC cylindrical shells based on the HSDT and von-Karman type nonlinear kinematics. Free vibration responses of the CNTRC beam is

* Corresponding author.
E-mail addresses: kulmanimehar@gmail.com (K. Mehar), call2subrat@gmail.com, pandask@nitrkl.ac.in (S.K. Panda).

http://dx.doi.org/10.1016/j.compstruct.2016.02.038
0263-8223/

Nomenclature

E_{11}, E_{22} and E_{33} effective Young's modulus of the composite flat panel in x, y and z direction respectively
E_{11}^{CNT} and E_{22}^{CNT} Young's modulus of the CNT in x and y direction respectively
E^m Young's modulus of the matrix
V_{CNT}^* total volume fraction of the CNT
ρ^m and ρ^{CNT} density of the matrix and the CNT
V_{CNT} and V_m effective volume fraction of the CNT and matrix
η_1, η_2 and η_3 effectiveness parameters of the CNT
υ_{11}^{CNT}, υ^m and υ_{12} Poisson's ration of the CNT, matrix and composite respectively.
$[T^L]$ and $[T^{NL}]$ linear and nonlinear thickness coordination matrix
$\{\sigma\}$ and $[\bar{Q}]$ stress vector and reduced stiffness matrix, respectively
N_i interpolating function of the 'ith' node
U total strain energy
$W_{\Delta T}$ total work done due to thermal load
T kinetic energy

studied by Lin and Xiang [25] using von-Karman's geometric nonlinearity. Yas and Samadi [26] investigated the free vibration and buckling behavior of the functionally graded SWCNTs reinforced composite flat panel resting on the elastic foundation using TBT. Mehrabadi et al. [27] examined the buckling behavior of functionally graded SWCNTs reinforced rectangular flat panel using the FSDT kinematic model. The FSDT kinematics is utilized by Kerur and Ghosh [28] to investigate the active control of the geometrically nonlinear transient responses of the laminated composite flat panel integrated with active fibre composite and PVDF layer. Lei et al. [29] presented the free vibration of FG-CNTRC cylindrical panels based on the FSDT shell theory using the element free kp-Ritz method. Alibeigloo and Liew [30] investigated the bending behavior of the FG-CNTRC rectangular flat panel with simply supported boundary conditions based on the 3D elasticity theory. Later, the low-velocity impact behavior of sandwich plates based on FSDT and HSDT model was investigated by Mohammadi et al. [31]. Szekrenyes [32] investigated the stress distribution on the delaminated orthotropic composite plates using Reddy's third-order shear deformation theory (TSDT). Wattanasakulpong et al. [33] analyzed the thermal buckling and the vibration behavior of the functionally graded beam using the TSDT kinematics. Ferreira et al. [34] reported the free vibration behavior of the functionally graded structure using the meshless method in the framework of the HSDT. Shen and Xiang [35] computed the nonlinear bending behavior of two type functionally graded CNTRC cylindrical panel

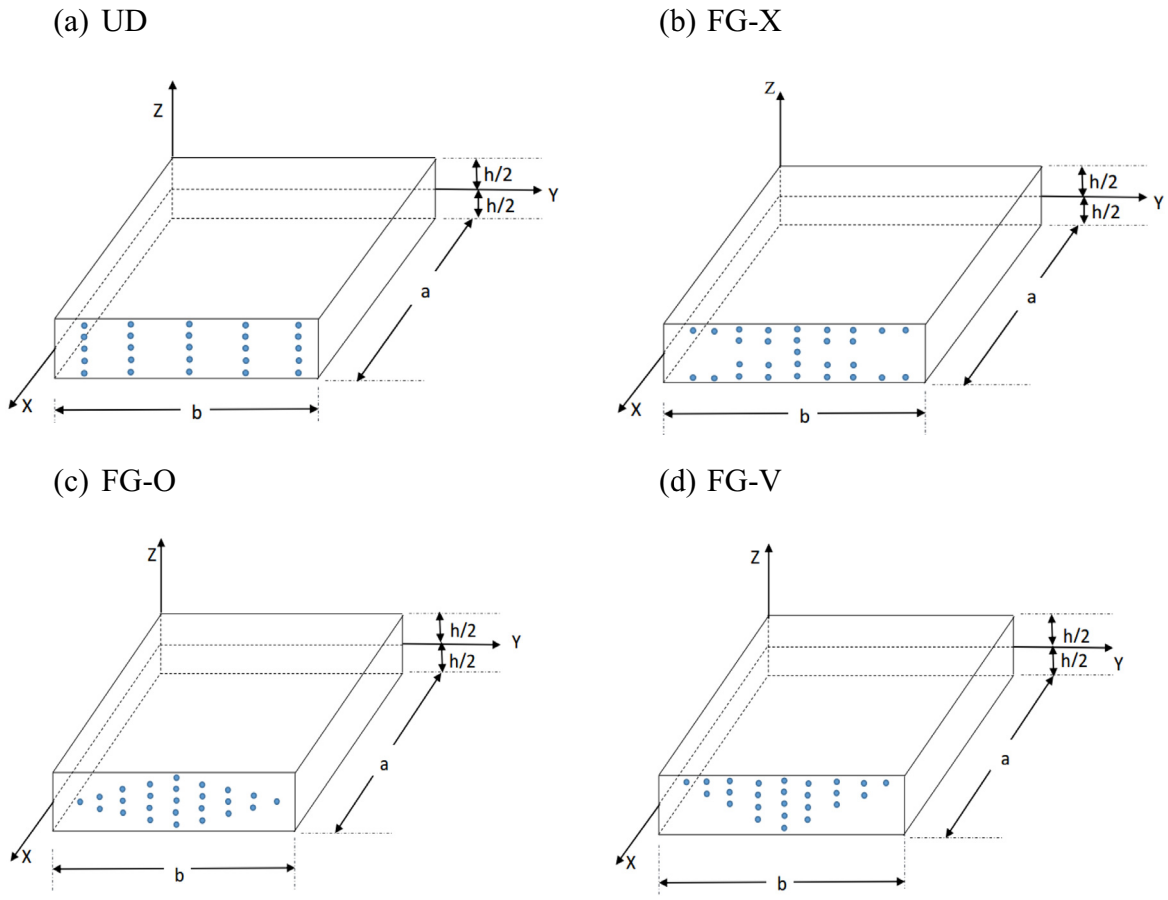

Fig. 1. The geometry and configuration of FG-CNTRC flat panels for different grading (a) UD, (b) FG-X, (c) FG-O and (d) FG-V.

resting on elastic foundation using von-Karman geometrical nonlinearity. Few studies are also focused on the method of solution for the computation using the numerical and semi-analytical methods. Lei et al. [36] reported the buckling responses of the FG-CNTRC flat panel based on the FSDT flat panel theory using the element free kp-Ritz method. Ayatollahi et al. [37] used a molecular model in conjunction with the finite element method (FEM) to compute the nonlinear mechanical properties of the armchair and the zigzag SWCNTs. Panigrahi and Zhang [38] computed the 3D stress of tee joint made by laminated composite using nonlinear FEM. Shi et al. [39] investigated the static and dynamic behavior of the space truss structures using FEM by considering geometrical and material nonlinearity of the structure. Free vibration behavior of the laminated FG-CNTRC plate investigated by Lei et al. [40] using the FSDT kinematics with the help of kp-Ritz method. Brischetto [41] used continuum approach to investigate the vibration behavior of the SWCNT. Tornabene et al. [42] investigated the effect of CNT agglomeration on the free vibration response of the FG-CNT reinforced laminated composite panel using the generalized differential quadrature (GDQ) method. A broad review of the mechanical behavior of the CNTRC is presented by Liew et al. [43]. Brischetto et al. [44] examined the free vibration behavior of the SWCNT and double wall carbon nanotube (DWCNT) using the refined 2D GDQ shell methods and an exact 3D shell model. Cinefra et al. [45] also incorporated the refined shell model to examine the vibration behavior of the DWCNT.

It is clear from the above review that the numerous attempts have already been made in the past to analyze the linear and nonlinear free vibration responses of the FG-CNTRC flat/curved panels based on available shear deformation and classical theories. However, we note that most of the works are based on the FSDT kinematics and von-Karman type nonlinear strain. Based on the author's knowledge, no study has been reported yet on the nonlinear free vibration behavior of the FG-CNTRC plate using the HSDT kinematics and Green-Lagrange nonlinear kinematics including the temperature dependent properties due to the uniform temperature rise. In this study, the authors aim to compute the nonlinear vibration behavior of the FG-CNTRC flat panel using the HSDT kinematics and Green-Lagrange nonlinearity under uniform thermal environment. The material properties of the FG-CNTRC flat panel are assumed to be temperature-dependent and graded using various grading rule through the thickness. The present model included all the nonlinear higher order terms to capture the exact strain under sever nonlinearity. The governing equation of the FG-CNTRCs flat panel is obtained using Hamilton's principle and discretized using a nine-noded quadrilateral Lagrangian element with nine degrees of freedom per node. The desired nonlinear frequency responses are computed using the direct iterative method [46]. Finally, the influence of the material and the geometrical parameters on the nonlinear frequency responses are highlighted by computing several numerical examples for the volume fractions, the thickness ratios and the support conditions under elevated thermal environment.

2. Theory and general formulation

For the investigation purpose, the FG-CNTRC flat panel configuration is considered, and the dimensions are, length a, width b and thickness h as shown in Fig. 1. The CNTs are assumed to align along the length of the panel. In this analysis four types of CNT configurations are assumed as in Fig. 1, namely, uniformly distributed (UD), FG-X (CNT volume fractions are higher at the top and the bottom surfaces of the plate), FG-O (CNT volume fractions are higher at the mid-plane) and FG-V (CNT volume fractions varies low to high from the bottom to the top surface of the plate). The mathematical expression of the effective volume fractions for each type of FG-CNT configurations are expressed as [23]:

$$V_{CNT}(z)=\left.\begin{cases} V^*_{CNT} & (UD)\\ 2\left(\frac{2|z|}{h}\right)V^*_{CNT} & (FG-X)\\ 2\left(1-\frac{2|z|}{h}\right)V^*_{CNT} & (FG-O)\\ \left(1+\frac{2z}{h}\right)V^*_{CNT} & (FG-V)\end{cases}\right\}= \tag{1}$$

or,

$$V^*_{CNT}=\frac{w_{CNT}}{w_{CNT}+\left(\frac{\rho^{CNT}}{\rho^m}\right)-\left(\frac{\rho^{CNT}}{\rho^m}\right)w^{CNT}}$$

where, V^*_{CNT} is the total volume fraction of CNT, w_{CNT} is the mass fraction of the CNT, and ρ^m and ρ^{CNT} are densities of the matrix and CNT respectively.

2.1. Kinematic model

The mathematical model of FG-CNTRC flat panel is developed using the higher-order mid-plane kinematics as [32]:

$$\left.\begin{aligned} u(x,y,z,t)&=u_0(x,y,t)+z\varphi_x(x,y,t)+z^2\psi_x(x,y,t)+z^3\theta_x(x,y,t)\\ v(x,y,z,t)&=v_0(x,y,t)+z\varphi_y(x,y,t)+z^2\psi_y(x,y,t)+z^3\theta_y(x,y,t)\\ w(x,y,z,t)&=w_0(x,y,t)\end{aligned}\right\} \tag{2}$$

where, u, v and w are the displacement of any point within the panel along x, y and z directions, respectively. u_0, v_0 and w_0 are the mid plane displacement of any point along x, y and z directions, respectively. φ_x and φ_y are the rotation of normal to the mid-plane about the y and x-axis, respectively. The functions ψ_x, ψ_y, θ_x and θ_y are higher order terms of Tayler series expansion in the mid-plane of the flat panel.

Now, the Eq. (2) is rearranged in the matrix form and conceded as:

$$\{\lambda\}=[f]\{\lambda_0\} \tag{3}$$

where, $\{\lambda\}$, $[f]$ and $\{\lambda_0\}$ are the global displacement vector of any point, thickness coordinate matrix, and nodal displacement vector within the mid-plane respectively. The details of each matrix and the vectors are provided in the Appendix (A.1).

2.2. Strain-displacement relations

The following equation defines the strain-displacement relation which is commonly known as Green-Lagrange strain for any general material continuum [47]

$$\{\varepsilon_{ij}\}=\begin{Bmatrix}\varepsilon_{xx}\\ \varepsilon_{yy}\\ \gamma_{xy}\\ \gamma_{zx}\\ \gamma_{yz}\end{Bmatrix}=\begin{Bmatrix}u_{,x}\\ v_{,y}\\ u_{,y}+v_{,x}\\ u_{,z}+w_{,x}\\ v_{,z}+w_{,y}\end{Bmatrix}+\begin{Bmatrix}\frac{1}{2}[(u_{,x})^2+(v_{,x})^2+(w_{,x})^2]\\ \frac{1}{2}[(u_{,y})^2+(v_{,y})^2+(w_{,y})^2]\\ u_{,x}u_{,y}+v_{,x}v_{,y}+w_{,x}w_{,y}\\ u_{,z}u_{,x}+v_{,z}v_{,x}+w_{,z}w_{,x}\\ u_{,z}u_{,y}+v_{,z}v_{,y}+w_{,z}w_{,y}\end{Bmatrix} \tag{4}$$

Eq. (4) can be rewritten in the further notation of the linear and the nonlinear strain in the following manner

$$\{\varepsilon_{ij}\}=\{\varepsilon_L\}+\{\varepsilon_{NL}\} \tag{5}$$

By substituting the values of the displacement field Eq. (4), the strain vector is expressed as:

$$\{\varepsilon_{ij}\}=\begin{Bmatrix}\varepsilon_{xx}\\ \varepsilon_{yy}\\ \gamma_{xy}\\ \gamma_{zx}\\ \gamma_{yz}\end{Bmatrix}=\begin{Bmatrix}\varepsilon_x^0\\ \varepsilon_y^0\\ \varepsilon_{xy}^0\\ \varepsilon_{zx}^0\\ \varepsilon_{yz}^0\end{Bmatrix}+\begin{Bmatrix}\varepsilon_x^4\\ \varepsilon_y^4\\ \varepsilon_{xy}^4\\ \varepsilon_{zx}^4\\ \varepsilon_{yz}^4\end{Bmatrix}+z\left\{\begin{Bmatrix}k_x^1\\ k_y^1\\ k_{xy}^1\\ k_{zx}^1\\ k_{yz}^1\end{Bmatrix}+\begin{Bmatrix}k_x^5\\ k_y^5\\ k_{xy}^5\\ k_{zx}^5\\ k_{yz}^5\end{Bmatrix}\right\}+z^2\left\{\begin{Bmatrix}k_x^2\\ k_y^2\\ k_{xy}^2\\ k_{zx}^2\\ k_{yz}^2\end{Bmatrix}+\begin{Bmatrix}k_x^6\\ k_y^6\\ k_{xy}^6\\ k_{zx}^6\\ k_{yz}^6\end{Bmatrix}\right\}+z^3\left\{\begin{Bmatrix}k_x^3\\ k_y^3\\ k_{xy}^3\\ k_{zx}^3\\ k_{yz}^3\end{Bmatrix}+\begin{Bmatrix}k_x^7\\ k_y^7\\ k_{xy}^7\\ k_{zx}^7\\ k_{yz}^7\end{Bmatrix}\right\}+z^4\begin{Bmatrix}k_x^8\\ k_y^8\\ k_{xy}^8\\ k_{zx}^8\\ k_{yz}^8\end{Bmatrix}+z^5\begin{Bmatrix}k_x^9\\ k_y^9\\ k_{xy}^9\\ k_{zx}^9\\ k_{yz}^9\end{Bmatrix}+z^6\begin{Bmatrix}k_x^{10}\\ k_y^{10}\\ k_{xy}^{10}\\ k_{zx}^{10}\\ k_{yz}^{10}\end{Bmatrix} \tag{6}$$

Eq. (6) can further be arranged as follows:

$$\{\varepsilon_{ij}\}=[\mathrm{T^L}]\{\bar{\varepsilon}_L\}+[\mathrm{T^{NL}}]\{\bar{\varepsilon}_{NL}\} \tag{7}$$

where $\{\bar{\varepsilon}_L\}=\{\varepsilon_x^0\ \varepsilon_y^0\ \varepsilon_{xy}^0\ \varepsilon_{zx}^0\ \varepsilon_{yz}^0\ k_x^1\ k_y^1\ k_{xy}^1\ k_{zx}^1\ k_{yz}^1\ k_x^2\ k_y^2\ k_{xy}^2\ k_{zx}^2\ k_{yz}^2\ k_x^3\ k_y^3\ k_{xy}^3\ k_{zx}^3\ k_{yz}^3\}^T$ and $\{\bar{\varepsilon}_{NL}\}=\{\varepsilon_x^4\ \varepsilon_y^4\ \varepsilon_{xy}^4\ \varepsilon_{zx}^4\ \varepsilon_{yz}^4\ k_x^5\ k_y^5\ k_{xy}^5\ k_{zx}^5\ k_{yz}^5\ k_x^6\ k_y^6\ k_{xy}^6\ k_{zx}^6\ k_{yz}^6\ k_x^7\ k_y^7\ k_{xy}^7\ k_{zx}^7\ k_{yz}^7\ k_x^8\ k_y^8\ k_{xy}^8\ k_{zx}^8\ k_{yz}^8\ k_x^9\ k_y^9\ k_{xy}^9\ k_{zx}^9\ k_{yz}^9\ k_x^{10}\ k_y^{10}\ k_{xy}^{10}\ k_{zx}^{10}\ k_{yz}^{10}\}^T$ are the linear and nonlinear mid-plane strain vectors and the individual terms are defined in Appendix (A.2). Similarly, $[\mathrm{T_L}]$ and $[\mathrm{T_{NL}}]$ are the linear and nonlinear thickness coordinate matrices and provided in Appendix (A.3).

2.3. Effective material properties

The effective material properties of the FG-CNTRC material is computed using the extended rule of mixture as [23]:

$$E_{11}=\eta_1 V_{CNT}E_{11}^{CNT}+V_m E^m \tag{8}$$

$$\frac{\eta_2}{E_{22}}=\frac{V_{CNT}}{E_{22}^{CNT}}+\frac{V_m}{E^m} \tag{9}$$

$$\frac{\eta_3}{G_{12}}=\frac{V_{CNT}}{G_{12}^{CNT}}+\frac{V_m}{G^m} \tag{10}$$

where, η_1, η_2 and η_3 are the effectiveness parameter. The CNT is the short fibre, therefore, the effectiveness parameters are utilized to calculate the effective material properties through the extended rule of mixture and it is because the short fiber does not obey the same rule as in the case of long fiber.

In this analysis, the total volume of the composite is taken as the individual contribution of the carbon nanotube and the polymer matrix volume fractions and expressed as [23]:

$$V_{CNT}+V_m=1 \tag{11}$$

Similarly, the effective Poisson's ratio (v_{12}) and the density of the FG-CNTRC material can be obtained using the following formula as [23]:

$$v_{12}=V_{CNT}v^{CNT}+V_m v^m \tag{12}$$

$$\rho=V_{CNT}\rho^{CNT}+V_m\rho^m \tag{13}$$

2.4. Constitutive relation

The constitutive relations for any general FG-CNT flat panel is expressed as:

$$\begin{Bmatrix}\sigma_{xx}\\ \sigma_{yy}\\ \tau_{xy}\\ \tau_{zx}\\ \tau_{yz}\end{Bmatrix}=\begin{bmatrix}Q_{11}&Q_{12}&0&0&0\\ Q_{21}&Q_{22}&0&0&0\\ 0&0&Q_{66}&0&0\\ 0&0&0&Q_{55}&0\\ 0&0&0&0&Q_{44}\end{bmatrix}\left(\begin{Bmatrix}\varepsilon_{xx}\\ \varepsilon_{yy}\\ \gamma_{xy}\\ \gamma_{zx}\\ \gamma_{yz}\end{Bmatrix}-\begin{Bmatrix}\alpha_{11}\\ \alpha_{22}\\ 0\\ 0\\ 0\end{Bmatrix}\Delta T\right) \tag{14}$$

where, $Q_{11}=E_{11}/(1-v_{12}v_{21})$, $Q_{12}=v_{12}E_{22}/(1-v_{12}v_{21})$, $Q_{22}=E_{22}/(1-v_{12}v_{21})$, $Q_{66}=G_{12}$, $Q_{44}=G_{13}$ and $Q_{55}=G_{23}$. In which we assumed that $G_{13}=G_{12}$ and $G_{23}=1.2\times G_{12}$. ΔT is the uniform temperature rise across the panel thickness.

Eq. (14) can also be rewritten as:

$$\{\sigma\}=[\bar{Q}]\{\varepsilon-\varepsilon_{th}\} \tag{15}$$

where, $[\bar{Q}]$ is the reduced stiffness matrix.

2.5. Strain energy

The total strain energy of the free vibrated FG-CNTRC flat panel can be expressed as:

$$U=\frac{1}{2}\int\int\left[\int_{+h/2}^{-h/2}\{\varepsilon\}^T\{\sigma\}dz\right]dxdy \tag{16}$$

where, h is the total thickness of the FG-CNTRC flat panel.

Now, Eq. (16) can be rewritten by substituting strains and stresses from Eqs. (4) and (15) and conceded as:

$$U=\frac{1}{2}\int_A\Big(\{\bar{\varepsilon}_l\}^T[D_1]\{\bar{\varepsilon}_L\}+\{\bar{\varepsilon}_L\}^T[D_2]\{\bar{\varepsilon}_{NL}\}+\{\bar{\varepsilon}_{NL}\}^T[D_3]\{\bar{\varepsilon}_L\}+\{\bar{\varepsilon}_{NL}\}^T[D_4]\{\bar{\varepsilon}_{NL}\}\Big)dA \tag{17}$$

where, $[D_1]=\int_{-h/2}^{+h/2}[T^L]^T[\bar{Q}][T^L]dz$, $[D_2]=\int_{-h/2}^{+h/2}[T^L]^T[\bar{Q}][T^{NL}]dz$, $[D_3]=\int_{-h/2}^{+h/2}[T^{NL}]^T[\bar{Q}][T^L]dz$ and $[D_4]=\int_{-h/2}^{+h/2}[T^{NL}]^T[\bar{Q}][T^{NL}]dz$.

2.6. Kinetic energy

The kinetic energy of the FG-CNTRC flat panel can be expressed as:

$$T=\frac{1}{2}\int_V\rho\{\dot{\lambda}\}^T\{\dot{\lambda}\}dV \tag{18}$$

where, ρ and $\{\dot{\lambda}\}$ are the mass density and the global velocity vector, respectively.

Using Eqs. (3) and (18), the kinetic energy of the FG-CNTRC flat panel with thickness h can be written as:

$$T=\frac{1}{2}\int_A\left(\int_{-h/2}^{+h/2}\{\dot{\lambda}_0\}^T[f]^T\rho[f]\{\dot{\lambda}_0\}dz\right)dA=\frac{1}{2}\int_A\{\dot{\lambda}_0\}^T[m]\{\dot{\lambda}_0\}dA \tag{19}$$

where, $[m]=\int_{-h/2}^{+h/2}[f]^T\rho[f]dz$ is the inertia matrix.

2.7. Work done due to thermal load

The in-plane thermal forces induced in the present FG-CNT flat panel due to the uniform thermal field can be obtained by integrating the stress equation over the thickness of the panel and it is expressed as:

$$\{N_{\Delta T}\} = \{N_x\ N_y\ N_{xy}\ 0\ 0\}^T = \int_{-h/2}^{h/2} [\bar{Q}]\{\alpha_x\ \alpha_y\ \alpha_{xy}\ 0\ 0\}^T \Delta T\, dz \tag{20}$$

where, N_x, N_y and N_{xy} are the in-plane thermal forces.

Now, the work done due to the in-plane thermal force $\{N_{\Delta T}\}$ and the corresponding geometrical distortion in Green-Lagrange for the flat panel can be expressed as [49]:

$$\{W_{\Delta T}\} = \int_V \begin{Bmatrix} \frac{1}{2}N_x[(u_{,x})^2 + (v_{,x})^2 + (w_{,x})^2] \\ +\frac{1}{2}N_y[(u_{,y})^2 + (v_{,y})^2 + (w_{,y})^2] \\ +N_{xy}[u_{,x}u_{,y} + v_{,x}v_{,y} + w_{,x}w_{,y}] \end{Bmatrix} dV \tag{21}$$

$$\{W_{\Delta T}\} = \int_V \begin{Bmatrix} u_{,x} \\ u_{,y} \\ v_{,x} \\ v_{,y} \\ w_{,x} \\ w_{,y} \end{Bmatrix}^T \begin{bmatrix} N_x & N_{xy} & 0 & 0 & 0 & 0 \\ N_{xy} & N_y & 0 & 0 & 0 & 0 \\ 0 & 0 & N_x & N_{xy} & 0 & 0 \\ 0 & 0 & N_{xy} & N_y & 0 & 0 \\ 0 & 0 & 0 & 0 & N_x & N_{xy} \\ 0 & 0 & 0 & 0 & N_{xy} & N_y \end{bmatrix} \begin{Bmatrix} u_{,x} \\ u_{,y} \\ v_{,x} \\ v_{,y} \\ w_{,x} \\ w_{,y} \end{Bmatrix} dV \tag{22}$$

$$\{W_{\Delta T}\} = \int\int \{\bar{\varepsilon}_G\}^T [D_G]\{\bar{\varepsilon}_G\} dxdy \tag{23}$$

where, $\{\bar{\varepsilon}_G\}$ is the geometric strain vector and $[D_G]$ is the material property matrix. where, $[D_G] = \int_{-h/2}^{h/2} [T_G]^T \begin{bmatrix} N_x & N_{xy} & 0 & 0 & 0 & 0 \\ N_{xy} & N_y & 0 & 0 & 0 & 0 \\ 0 & 0 & N_x & N_{xy} & 0 & 0 \\ 0 & 0 & N_{xy} & N_y & 0 & 0 \\ 0 & 0 & 0 & 0 & N_x & N_{xy} \\ 0 & 0 & 0 & 0 & N_{xy} & N_y \end{bmatrix} [T_G] dz$ and $[T_G]$ is thickness coordinate matrix same as $[T_L]$.

2.8. Finite element formulation

Finite element method is widely applied in worldwide for the numerical analysis of structures with geometrical and material complexities. In this present investigation, the domain is discretized using a nine-noded isoparametric quadrilateral Lagrangian element with nine degrees of freedom per node. Now, the mid-plane displacement of the desired field variables of the assumed displacement model $\{\lambda_0\}$ are expressed as follows:

$$\{\lambda_0\} = \sum_{i=1}^{9} N_i \{\lambda_{0i}\} \tag{24}$$

where, $\{\lambda_{0i}\} = [u_{0_i}\ v_{0_i}\ w_{0_i}\ \varphi_{x_i}\ \varphi_{y_i}\ \psi_{x_i}\ \psi_{y_i}\ \theta_{x_i}\ \theta_{y_i}]^T$ is the nodal displacement vector and N_i are the interpolating function of the 'ith' node.

The linear and nonlinear mid-plane strain vector in terms of nodal displacement vector can be written as

$$\{\bar{\varepsilon}_L\} = [B]\{\lambda_{0_i}\}, \quad \{\bar{\varepsilon}_G\} = [B_G]\{\lambda_{0_i}\}, \quad \{\bar{\varepsilon}_{NL}\} = [A][G]\{\lambda_{0_i}\} \tag{25}$$

where, $[B]$ and $[B_G]$ are the product form of differential operators and the shape functions for matices, respectively

$[A]$ is the function of displacements and $[G]$ is the product form of differential operator and shape functions in the nonlinear strain terms. The detail of $[B]$, $[B_G]$, $[A]$ and $[G]$ matrices are provided in the Appendices (A.4) and (A.5), respectively.

2.9. Governing equation

The governing equation of the FG-CNTRC flat panel is obtained using Hamilton's principle as:

$$\delta \int_{t_1}^{t_2} \{T - (U + W_{\Delta T})\} dt = 0 \tag{26}$$

Now the final form of nonlinear vibration governing equation of the FG-CNTRC flat panel is obtained by substituting the value of T, U, and $W_{\Delta T}$ in the Eq. (26) and conceded as:

$$[M]\{\ddot{\lambda}\} + ([K_L] + [K_G] + [K_{NL}]_1 + [K_{NL}]_2 + [K_{NL}]_3)\{\lambda\} = 0 \tag{27}$$

where, $[M] = [N]^T[m][N]$ is the system mass matrix, $[K_L] = [B]^T[D_1][B]$ is the linear stiffness matrix, $[K_G] = [B_G]^T[D_G][B_G]$ is the global geometrical stiffness matrix, $[K_{NL}]_1 = [B]^T[D_2][A][G]$ and $[K_{NL}]_2 = [G]^T[A]^T[D_3][B]$ are the coupled stiffness matrices (combination of linear and nonlinear strains) and $[K_{NL}]_3 = [G]^T[A]^T[D_4][A][G]$ is the nonlinear stiffness matrix.

Eq. (27) is now rewritten in the form of eigenvalue and eigenvector form and conceded as:

$$(([K_L] + [K_G] + [K_{NL}]_1 + [K_{NL}]_2 + [K_{NL}]_3) - \omega^2[M])\Delta = 0 \tag{28}$$

where, ω and Δ are the natural frequency and the corresponding eigenvector, respectively.

2.10. Solution technique

Now, the Eq. (28) has been solved by using the direct iterative method and the detailed procedures are mentioned in the following lines as [46]:

As a first step, the elemental stiffness and mass matrices are evaluated using the finite element steps.

a. Obtain the global stiffness and mass matrices by assembling the elemental matrices.
b. Now, solve the linear eigenvalue equation by dropping the nonlinear terms from the final governing equation.
c. Specify desired amplitude ratio ($Wmax/h$, where $Wmax$ is the maximum deflection at the center and h is the thickness of the flat panel) and the eigenvector is scaled up with the desired amplitude.
d. The nonlinear stiffness matrices are obtained using the scaled up eigenvector through the numerical integration.
e. Further, the nonlinear eigenvalue is computed by solving the governing equation for the nonlinear fundamental frequency.
f. The desired nonlinear response is obtained by repeating the step 3–5 until the desired convergence is obtained by setting the convergence criteria $\sqrt{(\bar{\omega}_n - \bar{\omega}_{n-1})^2/(\bar{\omega}_n)^2} \leqslant \chi$, here '$\chi$' and '$n$' denoted the convergence tolerance and iteration number, respectively.

3. Results and discussions

A customized computer code has been developed in MATLAB environment based on the present finite element micromechanical model for the evaluation of the nonlinear vibration behavior of FG-CNTRC flat panel under thermal environment. In the present analysis, PMMA is considered as the matrix materials and the temperature dependent material properties are considered as

Table 1
Material properties of SWCNT (10, 10) (L = 9.26 nm, R = 0.68 nm, h = 0.067 nm, v_{12}^{CNT} = 0.175).

Temperature (K)	E_{11}^{CNT} (TPa)	E_{22}^{CNT} (TPa)	G_{12}^{CNT} (TPa)	α_{11}^{CNT} (10^{-6}/K)	α_{22}^{CNT} (10^{-6}/K)
300	5.6466	7.0800	1.9445	3.4584	5.1682
400	5.5679	6.9814	1.9703	4.1496	5.0905
500	5.5308	6.9348	1.9643	4.5361	5.0189
700	5.4744	6.8641	1.9644	4.6677	4.8943

Table 2
Effectiveness parameter of the CNT.

V^*_{CNT}	η_1	η_2	η_3
0.12	0.137	1.022	0.715
0.17	0.142	1.626	1.138
0.28	0.141	1.585	1.109

$\rho = 1150\ \text{kg/m}^3$, $E^m = (3.52 - 0.0034T)$ GPa and $\alpha = 45(1 + 0.0005\Delta T) \times 10^{-6}$, where, $\Delta T = T - T_0$ and $T_0 = 300$ K (ambient temperature). Similarly, the SWCNTs of armchair (10, 10) configuration is considered as the reinforcement phase. The material properties of the SWCNT are taken from [21]. The effective properties and the effectiveness parameters of the SWCNT are provided in Tables 1 and 2, respectively.

The following sets of support conditions are used in the present analysis:

(a) All edges simply supported condition (SSSS):
$v = w = \varphi_y = \psi_y = \theta_y = 0$ at $x = 0, a$ and $u = w = \varphi_x = \psi_x = \theta_x = 0$ at $y = 0, b$
(b) All edges clamped condition (CCCC):
$u = v = w = \varphi_x = \varphi_y = \psi_x = \psi_y = \theta_x = \theta_y = 0$ for both $x = 0, a$ and $y = 0, b$.

In this analysis, the linear and nonlinear frequencies of the FG-CNTRC flat panel is nondimensionalized using the formula as: $\bar{\omega} = \omega(a^2/h)\sqrt{\rho_0/E_0}$, where, E_0 and ρ_0 are the Young's modulus and density of matrix at 300 K respectively.

3.1. Convergence and validation study

As a first step, the convergence behavior of the present nonlinear numerical model of the FG-CNTRC flat panel is computed for four different grading (UD, FG-X, FG-V, and FG-O) at ambient temperature (300 K) for different mesh division. The nondimensional linear and nonlinear frequency responses of the square FG-CNTRC flat panel are computed numerically under two support conditions (CCCC and SSSS) and presented in Figs. 2 and 3, respectively. For the computational purpose, other geometrical parameters are taken as $a/h = 50$ and $V^*_{CNT} = 0.11$. It is clearly observed from the figures that the present mathematical model is converging well with the mesh refinement for all different types of grading and support conditions. Based on the convergence, a (6×6) mesh is utilized to compute the further responses.

Now the proposed HSDT model is extended to show the validation behavior by comparing the nondimensional fundamental frequency parameters of square simply supported flat panel for different thickness ratios and presented in Table 3. The material properties and the geometrical parameters are taken from [23]. Similarly, the frequency ratios (ratio of nonlinear fundamental frequency to the linear frequency) are computed using the present higher-order model for the FG-CNTRC flat panels of two different gradings (UD and FG-V) and five amplitude ratios ($W_{max}/h = 0.2$,

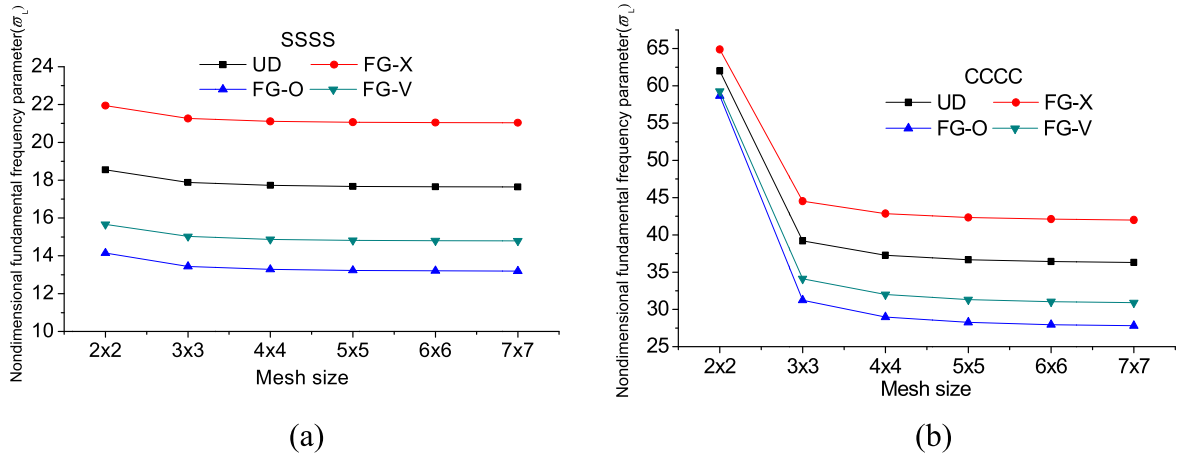

Fig. 2. Convergence study of linear frequency parameter of the FG-CNTRC flat panel.

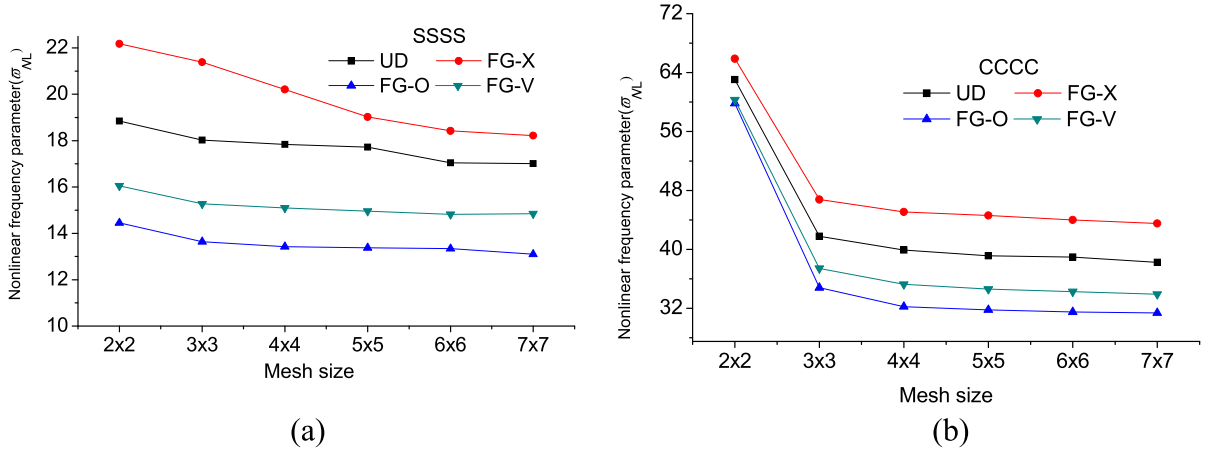

Fig. 3. Convergence study of nonlinear frequency parameter of the FG-CNTRC flat panel.

Table 3
Comparison study of nondimensional fundamental frequencies of square simply supported FG-CNTRC flat panel (V^*_{CNT} = 0.17, T = 300 K).

a/h	UD		FG-X		FG-O		FG-V	
	Present	[23]	Present	[23]	Present	[23]	Present	[23]
10	13.553	13.532	14.679	14.616	11.316	11.550	12.150	12.452
20	17.322	17.355	19.920	19.939	13.405	13.523	14.833	15.110
50	19.203	19.223	22.945	22.984	14.291	14.302	16.046	16.252

Table 4
Comparison study of frequency ratios ($\bar{\omega}_{NL}/\bar{\omega}_L$) of square FG-CNTRC flat panel (V^*_{CNT} = 0.17, T = 300 K and a/h = 100).

Grading	Sources	$\bar{\omega}_L$	W_{max}/h				
			0.2	0.4	0.6	0.8	1.0
UD	Present	21.7719	1.0106	1.0420	1.0932	1.1692	1.2472
	[23]	21.6989	1.0322	1.1232	1.2603	1.4304	1.6231
FG-V	Present	20.6175	1.0787	1.1714	1.2768	1.3900	1.5117
	[23]	18.2103	1.0454	1.1711	1.3549	1.5766	1.8224

0.4, 0.6, 0.8 and 1.0). It is well known that the flat panels are the simplest form of the curved panel. The responses are computed using the same geometrical and the material properties same as in [48] and presented in Table 4. It is clearly observed that the present results are showing good agreement with that of the reference with noticeable differences for the higher amplitude ratios. The differences between the results indicate the effect of Green-Lagrange type nonlinear kinematics in the framework of the HSDT instead of the von-Karman nonlinearity for the analysis of any graded structure when exposed to severe nonlinearity.

3.2. Parametric study

Based on the convergence and comparison study now the newly developed nonlinear micromechanical higher-order finite element model of FG-CNTRC flat panel is extended to show the effect of different geometrical and material parameters on the nonlinear vibration behavior. In general, the responses are computed for four types of square FG-CNTRC flat panel (UD, FG-X, FG-O and FG-V) by taking a/h = 50 and V^*_{CNT} = 0.12 at 300 K throughout the analysis, if not stated otherwise. For the computational purpose, the FG-CNTRC panel thickness is taken to be h = 0.002 m throughout the analysis.

It is well known that the volume fractions of the filler material play a major role in the fabrication and the stiffness behavior of the polymer-based composites. Therefore in this example the effect of three volume fractions (V^*_{CNT} = 0.12, 0.17 and 0.28) on the nonlinear vibration behavior of the FG-CNTRC flat panel is investigated under two support conditions (SSSS and CCCC) and six amplitude ratios (W_{max}/h = 0.25, 0.5, 0.75, 1.0, 1.25 and 1.5). The responses are presented in Table 5 and observed that the nondimensional fundamental frequency increases as the CNT volume fractions increase. The fundamental frequency parameters are also observed maximum and minimum for the FG-X and FG-O type FG-CNTRC flat panel, respectively. It is because, the CNT volume fractions are maximum at the top and bottom surfaces of the FG-X type FG-CNTRC panel whereas minimum for FG-O type (CNT volume fractions are higher at mid-plane). It is also observed that the nonlinear frequency parameters are increasing as the amplitude ratio increases except few cases. The non-monotonous behavior of the frequency responses is observed for higher amplitude ratio, i.e., $W_{max}/h \geqslant 1.0$ may be due to the inclusion of all the nonlinear higher order terms in the present mathematical model.

Table 6 shows the effect of thickness ratios on the linear and nonlinear frequency responses of FG-CNTRC flat-panel. The

Table 5
Effect of the volume fraction and amplitude ratio on the non-dimensionalized nonlinear frequency parameter of the FG-CNTRC flat panel.

Support conditions	V^*_{CNT}	Grading	W_{max}/h						
			0	0.25	0.50	0.75	1.00	1.25	1.50
CCCC	0.12	UD	36.426	36.645	36.995	36.729	39.384	39.918	41.561
		FG-X	42.114	42.201	42.443	43.391	44.374	43.014	41.117
		FG-O	27.960	28.173	28.850	29.981	31.497	33.383	35.463
		FG-V	31.045	31.197	31.963	32.942	33.570	33.616	34.470
	0.17	UD	44.525	44.728	45.208	46.227	47.320	48.466	50.360
		FG-X	51.672	51.843	52.351	53.189	54.340	55.847	57.640
		FG-O	34.014	34.290	35.101	36.449	38.277	40.443	43.069
		FG-V	37.635	37.900	38.457	39.395	41.439	40.150	40.987
	0.28	UD	53.467	53.678	54.385	55.462	57.211	59.062	60.848
		FG-X	61.216	61.358	61.759	63.069	64.676	64.485	64.254
		FG-O	41.238	41.578	42.556	44.322	46.676	49.433	52.507
		FG-V	44.995	45.233	46.343	47.829	48.955	47.787	48.381
SSSS	0.12	UD	17.656	17.653	17.563	17.393	16.615	16.706	15.494
		FG-X	21.049	21.012	20.665	19.040	17.996	17.838	17.701
		FG-O	13.209	13.217	13.240	13.268	13.300	13.303	13.308
		FG-V	14.798	14.803	14.811	14.853	14.877	14.876	14.796
	0.17	UD	21.391	21.393	21.316	21.109	20.815	20.468	19.016
		FG-X	25.545	25.512	25.198	24.143	22.661	23.123	22.235
		FG-O	15.975	15.988	16.024	16.086	16.171	16.280	16.411
		FG-V	17.824	17.844	17.872	17.918	17.993	18.112	17.944
	0.28	UD	26.316	26.312	26.073	24.187	24.047	22.875	22.646
		FG-X	31.473	31.438	31.483	27.636	27.694	26.245	24.970
		FG-O	19.436	19.447	19.476	19.475	25.777	19.258	19.025
		FG-V	21.594	21.611	21.650	21.714	21.807	21.873	21.943

Table 6
Effect of thickness ratio on the non-dimensionalized nonlinear frequency of the FG-CNTRC flat panel.

Support conditions	a/h	Grading	W_{max}/h						
			0	0.25	0.50	0.75	1.00	1.25	1.50
CCCC	50	UD	36.426	36.645	36.995	36.729	39.384	39.918	41.561
		FG-X	42.114	42.201	42.443	43.391	44.374	43.014	41.117
		FG-O	27.960	28.173	28.850	29.981	31.497	33.383	35.463
		FG-V	31.045	31.197	31.963	32.942	33.570	33.616	34.470
	100	UD	39.824	40.113	40.485	41.325	42.476	43.946	45.377
		FG-X	47.383	47.491	47.815	48.584	49.453	50.881	52.289
		FG-O	29.721	29.822	30.638	31.760	33.301	35.161	37.338
		FG-V	33.343	33.537	34.111	35.104	36.393	38.082	40.099
SSSS	50	UD	17.656	17.653	17.563	17.393	16.615	16.706	15.494
		FG-X	21.049	21.012	20.665	19.040	17.996	17.838	17.701
		FG-O	13.209	13.217	13.240	13.268	13.300	13.303	13.308
		FG-V	14.798	14.803	14.811	14.853	14.877	14.876	14.796
	100	UD	18.011	18.018	18.041	18.081	18.138	18.169	18.235
		FG-X	21.638	21.685	21.820	21.687	21.724	21.773	21.832
		FG-O	13.380	13.454	13.415	13.459	13.520	13.598	13.692
		FG-V	15.028	15.049	15.085	15.137	15.203	15.285	15.370

Table 7
Effect of temperature on the non-dimensionalized nonlinear frequency the of FG-CNTRC flat panel.

Support Conditions	T (K)	Grading	W_{max}/h						
			0	0.25	0.50	0.75	1.00	1.25	1.50
CCCC	300	UD	36.426	36.645	36.995	36.729	39.384	39.918	41.561
		FG-X	42.114	42.201	42.443	43.391	44.374	43.014	41.117
		FG-O	27.960	28.173	28.850	29.981	31.497	33.383	35.463
		FG-V	31.045	31.197	31.963	32.942	33.570	33.616	34.470
	500	UD	34.542	34.710	34.576	35.305	35.739	37.494	39.111
		FG-X	39.618	39.759	40.185	40.894	41.890	43.191	44.624
		FG-O	26.612	26.840	27.518	28.626	30.153	31.962	33.741
		FG-V	29.484	29.722	30.385	31.463	31.879	33.304	30.779
SSSS	300	UD	17.656	17.653	17.563	17.393	16.615	16.706	15.494
		FG-X	21.049	21.012	20.665	19.040	17.996	17.838	17.701
		FG-O	13.209	13.217	13.240	13.268	13.300	13.303	13.308
		FG-V	14.798	14.803	14.811	14.853	14.877	14.876	14.796
	500	UD	17.108	17.087	16.864	15.598	14.801	15.355	13.575
		FG-X	20.400	20.274	18.907	18.458	16.981	17.492	17.328
		FG-O	12.706	12.706	12.719	12.707	12.661	12.339	12.045
		FG-V	14.263	14.270	14.252	14.058	13.730	13.502	13.141

responses are computed for two thickness ratios ($a/h = 50$ and 100), six amplitude ratios ($W_{max}/h = 0.25$, 0.5, 0.75, 1.0, 1.25 and 1.5) under two support conditions (CCCC and SSSS). It is observed that the nondimensional fundamental frequency responses of the FG-CNTRC flat panel increases as the thickness ratio and the amplitude ratio increases. The non-dimensional linear frequency parameters are minimum and maximum for the FG-O and FG-X type of the FG-CNTRC panel, respectively, and the responses are within the expected line.

The CNT is well known for its good thermal property, and it becomes more important when the structure is exposed to elevated temperature field. In this present investigation, the CNT properties are assumed to temperature dependent, therefore, environment temperature plays a significant role on the vibration behavior of the FG-CNTRC flat panel. The nonlinear frequency responses of the square FG-CNTRC flat panel is computed for two different temperature ($T = 300$ K and 500 K), two support conditions (SSSS and CCCC) and presented in Table 7. It can be clearly observed that the nonlinear frequency responses of the FG-CNTRC flat panel increases as the amplitude ratios increase, however, decreases with the temperature load. It is because of the fact that the structural stiffness lowers as the temperature load increases and the responses follow the expected line.

4. Conclusions

In this study, the nonlinear free vibration behavior of the SWCNT reinforced composite flat panel of four different grading (UD, FG-X, FG-O, and FG-V) under uniform thermal environment have been examined using the HSDT kinematic model and Green-Lagrange nonlinearity. In addition, all the nonlinear higher-order terms are included in the mathematical model to achieve the exact flexure of the structure. The structure is graded functionally through the thickness based on the volume fractions of the CNT, and the effective properties are evaluated through the micromechanical model using the extended rule of mixture. To achieve the realistic behavior, the properties of CNT are considered to be temperature dependent. The desired governing equation for the vibration analysis is obtained using Hamilton's principle and discretized through the suitable isoparametric finite element steps. The desired responses are computed numerically using the direct iterative method. The convergence behavior of the present numerical higher-order model has been checked. The model has also been validated by comparing the responses to results available in the literature. The applicability of the present higher-order model has been highlighted by computing the responses for the different geometrical and material parameters and temperature

load as well. The following conclusions are drawn from the detailed parametric study.

(a) The convergence and the comparison studies indicated the accuracy of the present nonlinear HSDT model with and without thermal load.
(b) It is observed that the nonlinear frequency responses are decreasing with the increase of the temperature load because the stiffness of the FG-CNTRC panel decreases with temperature. However, the structural responses are following a reverse trend for the volume fractions and the thickness ratios.
(c) The results also clearly indicate that the FG-CNTRC flat-panel with FG-X type grading is a stiffer configuration than any of the other three made by different types of grading.

Appendix A

$$\{\lambda\} = \{u\ v\ w\}^T$$

$$\{\lambda_0\} = [u_0\ v_0\ w_0\ \varphi_x\ \varphi_y\ \psi_x\ \psi_y\ \theta_y\ \theta_x]^T$$

$$[f] = \begin{bmatrix} 1 & 0 & 0 & z & 0 & z^2 & 0 & z^3 & 0 \\ 0 & 1 & 0 & 0 & z & 0 & z^2 & 0 & z^3 \\ 0 & 0 & 1 & 0 & 0 & 0 & 0 & 0 & 0 \end{bmatrix} \tag{A.1}$$

$$\varepsilon_x^0 = u_{,x},\quad \varepsilon_y^0 = v_{,y},\quad \gamma_{xy}^0 = u_{,y} + v_{,x},\quad \gamma_{xz}^0 = \varphi_x + w_{,x},\quad \gamma_{yz}^0 = \varphi_y + w_{,y},$$

$$k_x^1 = \varphi_{x,x},\quad k_y^1 = \varphi_{y,y},\quad k_{xy}^1 = \varphi_{x,y} + \varphi_{y,x},\quad k_{zx}^1 = 2\psi_x,\quad k_{yz}^1 = 2\psi_y,$$

$$k_x^2 = \psi_{x,x},\quad k_y^2 = \psi_{y,y},\quad k_{xy}^2 = \psi_{x,y} + \psi_{y,x},\quad k_{zx}^2 = 3\theta_x,\quad k_{yz}^2 = 3\theta_y,$$

$$k_x^3 = \theta_{x,x},\quad k_y^3 = \theta_{y,y},\quad k_{xy}^3 = \theta_{x,y} + \theta_{y,x},\quad k_{zx}^3 = -\theta_x,\quad k_{yz}^3 = -\theta_y,$$

$$\varepsilon_x^4 = \left[(u_{,x})^2 + (v_{,x})^2 + (w_{,x})^2\right]$$

$$(\varepsilon_y^4) = \left[(u_{,y})^2 + (v_{,y})^2 + (w_{,y})^2\right]$$

$$\gamma_{xy}^4 = 2[u_{,x}u_{,y} + v_{,x}v_{,y} + w_{,x}w_{,y}]$$

$$\gamma_{zx}^4 = 2[\varphi_x u_{,x} + \varphi_y v_{,x}]$$

$$\gamma_{yz}^4 = 2[\varphi_x u_{,y} + \varphi_y v_{,y}]$$

$$(k_x^5) = 2[\varphi_{x,x}u_{,x} + \varphi_{y,x}v_{,x}],$$

$$(k_y^5) = 2[\varphi_{x,y}u_{,y} + \varphi_{y,y}v_{,y}],$$

$$(k_{xy}^5) = 2[\varphi_{x,y}u_{,x} + \varphi_{x,x}u_{,y} + 2\varphi_{y,x}v_{,y} + \varphi_{y,y}v_{,x}],$$

$$(k_{zx}^5) = 2[\varphi_x\varphi_{x,x} + 2\psi_x u_{,x} + \varphi_y\varphi_{y,x} + 2\psi_y v_{,x}],$$

$$(k_{yz}^5) = 2[\varphi_x\varphi_{x,y} + 2\psi_x u_{,y} + \varphi_y\varphi_{y,y} + 2\psi_y v_{,y}],$$

$$(k_x^6) = [\varphi_{x,x}^2 + \varphi_{y,x}^2 + 2\psi_{x,x}u_{,x} + 2\psi_{y,x}v_{,x}],$$

$$(k_y^6) = [\varphi_{x,y}^2 + \varphi_{y,y}^2 + 2\psi_{x,y}u_{,y} + 2\psi_{y,y}v_{,y}],$$

$$(k_{xy}^6) = 2[\varphi_{x,x}\varphi_{x,x} + \varphi_{y,x}\varphi_{y,y} + \psi_{x,x}u_{,y} + \psi_{x,x}u_{,y} + \psi_{y,x}v_{,y} + \psi_{y,y}v_{,x}],$$

$$(k_{zx}^6) = 2[\psi_{x,x}\varphi_x + \psi_{y,x}\varphi_y + 2\varphi_{x,x}\psi_x + 2\varphi_{y,x}\psi_y + 3u_{,x}\theta_x + 3v_{,x}\theta_y],$$

$$(k_{yz}^6) = 2[\psi_{x,y}\varphi_x + \psi_{y,y}\varphi_y + 2\varphi_{x,y}\psi_x + 2\varphi_{y,y}\psi_y + 3u_{,y}\theta_x + 3v_{,y}\theta_y],$$

$$(k_x^7) = 2[u_{,x}\theta_{x,x} + v_{,x}\theta_{y,x} + \varphi_{x,x}\psi_{x,x} + \varphi_{y,x}\psi_{y,x}],$$

$$(k_y^7) = 2[u_{,y}\theta_{x,y} + v_{,y}\theta_{y,y} + \varphi_{x,y}\psi_{x,y} + \varphi_{y,y}\psi_{y,y}],$$

$$(k_{xy}^7) = 2[u_{,x}\theta_{x,y} + u_{,y}\theta_{x,x} + v_{,x}\theta_{y,y} + v_{,y}\theta_{y,x} + \varphi_{x,x}\psi_{x,y} + \varphi_{x,y}\psi_{x,x} + \varphi_{y,x}\psi_{y,y} + \varphi_{y,y}\psi_{y,x}],$$

$$(k_{zx}^7) = 2[\theta_{x,x}\varphi_x + \theta_{y,x}\varphi_y + 2\psi_{x,x}\psi_x + 2\psi_{y,x}\psi_y + 3\varphi_{x,x}\theta_x + 3\varphi_{y,x}\theta_y],$$

$$(k_{yz}^7) = 2[\varphi_x\theta_{x,y} + \varphi_x\theta_{y,y} + 2\psi_x\psi_{x,y} + 2\psi_y\psi_{y,y} + 3\theta_x\varphi_{x,y} + 3\theta_y\varphi_{y,y}],$$

$$(k_x^8) = [\psi_{x,x}^2 + \psi_{y,x}^2 + 2\varphi_{x,x}\theta_{x,x} + 2\varphi_{y,x}\theta_{y,x}],$$

$$(k_y^8) = [\psi_{x,y}^2 + \psi_{y,y}^2 + 2\varphi_{x,y}\theta_{x,y} + 2\varphi_{y,y}\theta_{y,y}],$$

$$(k_{xy}^8) = [\psi_{x,x}\psi_{x,y} + \psi_{y,x}\psi_{y,y} + 2\theta_{x,x}\varphi_{x,y} + 2\theta_{y,x}\varphi_{y,y} + 2\theta_{x,x}\varphi_{x,x} + 2\theta_{y,x}\varphi_{y,x}],$$

$$(k_{zx}^8) = 2[2\psi_x\theta_{x,x} + 2\psi_y\theta_{y,x} + 3\theta_x\psi_{x,x} + 3\theta_y\psi_{y,x}],$$

$$(k_{yz}^8) = 2[2\psi_x\theta_{x,y} + 2\psi_y\theta_{y,y} + 3\theta_x\psi_{x,y} + 3\theta_x\psi_{x,y}],$$

$$(k_x^9) = 2[\psi_{x,x}\theta_{x,x} + \psi_{y,x}\theta_{y,x}],$$

$$(k_y^9) = 2[\psi_{x,y}\theta_{x,y} + \psi_{y,y}\theta_{y,y}],$$

$$(k_{xy}^9) = 2[\psi_{x,x}\theta_{x,y} + \psi_{y,x}\theta_{y,y} + \theta_{x,x}\psi_{x,y} + \theta_{y,x}\psi_{y,y}],$$

$$(k_{zx}^9) = 2[3\theta_x\theta_{x,x} + 3\theta_y\theta_{y,x}],$$

$$(k_{yz}^9) = [6(\theta_x\theta_{x,y} + \theta_y\theta_{y,y})],$$

$$(k_x^{10}) = [\theta_{x,x}^2 + \theta_{y,x}^2],$$

$$(k_y^{10}) = [\theta_{x,y}^2 + \theta_{y,y}^2],$$

$$(k_{xy}^{10}) = 2[\theta_{x,x}\theta_{x,y} + \theta_{y,x}\theta_{y,y}],$$

$$k_{zx}^{10} = 0,\ k_{yz}^{10} = 0.$$

Some coupled terms in the above equations

$$u_{,x} = \frac{\partial u_0}{\partial x},\quad v_{,y} = \frac{\partial v_0}{\partial y},\quad u_{,y} = \frac{\partial u_0}{\partial y},\quad v_{,x} = \frac{\partial v_0}{\partial x},\quad w_{,x} = \frac{\partial w_0}{\partial x},$$

$$w_{,y} = \frac{\partial w_0}{\partial y},\quad \varphi_{y,y} = \frac{\partial \varphi_y}{\partial y},\quad \varphi_{x,y} = \frac{\partial \varphi_x}{\partial y},\quad \varphi_{y,x} = \frac{\partial \varphi_y}{\partial x},$$

$$\psi_{x,x} = \frac{\partial \psi_x}{\partial x},\quad \psi_{y,y} = \frac{\partial \psi_y}{\partial y},\quad \psi_{x,y} = \frac{\partial \psi_x}{\partial y},\quad \psi_{y,x} = \frac{\partial \psi_y}{\partial x},$$

$$\theta_{x,x} = \frac{\partial \theta_x}{\partial x},\quad \theta_{y,y} = \frac{\partial \theta_y}{\partial y},\quad \theta_{x,y} = \frac{\partial \theta_x}{\partial y},\quad \theta_{y,x} = \frac{\partial \theta_y}{\partial x} \tag{A.2}$$

Linear and nonlinear thickness coordinate matrix

$$[T_L] = \begin{bmatrix} 1 & 0 & 0 & 0 & 0 & z & 0 & 0 & 0 & 0 & z^2 & 0 & 0 & 0 & 0 & z^3 & 0 & 0 & 0 & 0 \\ 0 & 1 & 0 & 0 & 0 & 0 & z & 0 & 0 & 0 & 0 & z^2 & 0 & 0 & 0 & 0 & z^3 & 0 & 0 & 0 \\ 0 & 0 & 1 & 0 & 0 & 0 & 0 & z & 0 & 0 & 0 & 0 & z^2 & 0 & 0 & 0 & 0 & z^3 & 0 & 0 \\ 0 & 0 & 0 & 1 & 0 & 0 & 0 & 0 & z & 0 & 0 & 0 & 0 & z^2 & 0 & 0 & 0 & 0 & z^3 & 0 \\ 0 & 0 & 0 & 0 & 1 & 0 & 0 & 0 & 0 & z & 0 & 0 & 0 & 0 & z^2 & 0 & 0 & 0 & 0 & z^3 \end{bmatrix}$$

$$[T_{NL}] = \begin{bmatrix} 1 & 0 & 0 & 0 & 0 & z & 0 & 0 & 0 & 0 & z^2 & 0 & 0 & 0 & 0 & z^3 & 0 & 0 & 0 & 0 & z^4 & 0 & 0 & 0 & 0 & z^5 & 0 & 0 & 0 & 0 & z^6 & 0 & 0 & 0 & 0 \\ 0 & 1 & 0 & 0 & 0 & 0 & z & 0 & 0 & 0 & 0 & z^2 & 0 & 0 & 0 & 0 & z^3 & 0 & 0 & 0 & 0 & z^4 & 0 & 0 & 0 & 0 & z^5 & 0 & 0 & 0 & 0 & z^6 & 0 & 0 & 0 \\ 0 & 0 & 1 & 0 & 0 & 0 & 0 & z & 0 & 0 & 0 & 0 & z^2 & 0 & 0 & 0 & 0 & z^3 & 0 & 0 & 0 & 0 & z^4 & 0 & 0 & 0 & 0 & z^5 & 0 & 0 & 0 & 0 & z^6 & 0 & 0 \\ 0 & 0 & 0 & 1 & 0 & 0 & 0 & 0 & z & 0 & 0 & 0 & 0 & z^2 & 0 & 0 & 0 & 0 & z^3 & 0 & 0 & 0 & 0 & z^4 & 0 & 0 & 0 & 0 & z^5 & 0 & 0 & 0 & 0 & z^6 & 0 \\ 0 & 0 & 0 & 0 & 1 & 0 & 0 & 0 & 0 & z & 0 & 0 & 0 & 0 & z^2 & 0 & 0 & 0 & 0 & z^3 & 0 & 0 & 0 & 0 & z^4 & 0 & 0 & 0 & 0 & z^5 & 0 & 0 & 0 & 0 & z^6 \end{bmatrix} \quad (A.3)$$

Individual terms of matrix $[B]$

$$[B]_{1,1} = \partial/\partial x,\ [B]_{2,2} = \partial/\partial y,\ [B]_{3,1} = \partial/\partial y,\ [B]_{3,2} = \partial/\partial x,$$
$$[B]_{4,3} = \partial/\partial x,\ [B]_{4,4} = 1, [B]_{5,3} = \partial/\partial x,\ [B]_{5,5} = 1,\ [B]_{6,4} = \partial/\partial x,$$
$$[B]_{7,5} = \partial/\partial y,\ [B]_{8,4} = \partial/\partial y,\ [B]_{8,5} = \partial/\partial x,\ [B]_{9,6} = 2,$$
$$[B]_{10,7} = 2,\ [B]_{11,6} = \partial/\partial x,\ [B]_{12,7} = \partial/\partial y,\ [B]_{13,6} = \partial/\partial y,$$
$$[B]_{13,7} = \partial/\partial x,\ [B]_{14,8} = 2,\ [B]_{15,9} = 2,\ [B]_{16,8} = \partial/\partial x,$$
$$[B]_{17,9} = \partial/\partial y,\ [B]_{18,8} = \partial/\partial y,\ [B]_{18,9} = \partial/\partial x.$$

Individual terms of matrix $[B_G]$

$$[B_G]_{1,1} = \partial/\partial x,\ [B_G]_{2,1} = \partial/\partial y,\ [B_G]_{3,2} = \partial/\partial x,\ [B_G]_{4,2} = \partial/\partial y,$$
$$[B_G]_{5,3} = \partial/\partial x,\ [B_G]_{6,3} = \partial/\partial y,\ [B_G]_{7,4} = \partial/\partial x,\ [B_G]_{8,4} = \partial/\partial y,$$
$$[B_G]_{9,5} = \partial/\partial x,\ [B_G]_{10,5} = \partial/\partial y,\ [B_G]_{13,6} = \partial/\partial x,\ [B_G]_{14,6} = \partial/\partial y,$$
$$[B_G]_{15,7} = \partial/\partial x,\ [B_G]_{16,7} = \partial/\partial y,\ [B_G]_{19,8} = \partial/\partial x,\ [B_G]_{20,8} = \partial/\partial y,$$
$$[B_G]_{21,9} = \partial/\partial x,\ [B_G]_{22,9} = \partial/\partial y. \quad (A.4)$$

Individual terms of matrix $[A]$

$$[A]_{1,1} = 1/2u_{,x},\ [A]_{1,3} = 1/2v_{,x},\ [A]_{1,5} = 1/2w_{,x},\ [A]_{2,2} = 1/2u_{,y},$$
$$[A]_{2,4} = 1/2v_{,y},\ [A]_{2,6} = 1/2w_{,y},\ [A]_{3,1} = u_{,y},\ [A]_{3,3} = v_{,y},$$
$$[A]_{3,5} = w_{,y},\ [A]_{4,1} = \varphi_x,\ [A]_{4,3} = \varphi_y,\ [A]_{5,2} = \varphi_x,\ [A]_{5,4} = \varphi_y,$$
$$[A]_{6,1} = \varphi_{x,x},\ [A]_{6,3} = \varphi_{y,x},\ [A]_{7,2} = \varphi_{x,y},\ [A]_{7,4} = \varphi_{y,y},\ [A]_{8,1} = \varphi_{x,y},$$
$$[A]_{8,2} = \varphi_{x,x},\ [A]_{8,3} = \varphi_{y,y},\ [A]_{8,4} = \varphi_{y,x},\ [A]_{9,1} = 2\psi_x,\ [A]_{9,3} = 2\psi_y,$$
$$[A]_{9,7} = \varphi_x,\ [A]_{9,9} = \varphi_y,\ [A]_{10,2} = 2\psi_x,\ [A]_{10,4} = 2\psi_y,\ [A]_{10,8} = \varphi_x,$$
$$[A]_{10,10} = \varphi_y,\ [A]_{11,1} = \psi_{x,x},\ [A]_{11,3} = \psi_{y,x},\ [A]_{11,7} = 1/2\varphi_{x,x},$$
$$[A]_{11,9} = 1/2\varphi_{y,x},\ [A]_{12,2} = \psi_{x,y},\ [A]_{12,4} = \psi_{y,y},\ [A]_{12,8} = 1/2\varphi_{x,y},$$
$$[A]_{12,10} = 1/2\varphi_{y,y},\ [A]_{13,1} = \psi_{x,y},\ [A]_{13,2} = \psi_{x,y},\ [A]13,3 = \psi_{y,y},$$
$$[A]_{13,4} = \psi_{y,x},\ [A]_{13,7} = \varphi_{x,y},\ [A]_{13,9} = \varphi_{y,y},\ [A]_{14,1} = 3\theta_x,$$
$$[A]_{14,3} = 3\theta_y,\ [A]_{14,7} = 2\psi_x,\ [A]_{14,9} = 2\psi_y,\ [A]_{14,11} = \varphi_x,\ [A]_{14,13} = \varphi_y,$$
$$[A]_{15,2} = 3\theta_x,\ [A]_{15,4} = 3\theta_y,\ [A]_{15,8} = 2\psi_x,\ [A]_{15,10} = 2\psi_y,$$
$$[A]_{15,12} = \varphi_x,\ [A]_{15,14} = \varphi_y,\ [A]_{16,1} = \theta_{x,x},\ [A]_{16,3} = \theta_{y,x},\ [A]_{16,7} = \psi_{x,x},$$
$$[A]_{16,9} = \psi_{y,x},\ [A]_{17,2} = \theta_{x,y},\ [A]_{17,4} = \theta_{y,y},\ [A]_{17,8} = \psi_{x,y},\ [A]_{17,10} = \psi_{y,y},$$
$$[A]_{18,1} = \theta_{x,y},\ [A]_{18,2} = \theta_{x,x},\ [A]_{18,3} = \theta_{y,y},\ [A]_{18,4} = \theta_{y,x},\ [A]_{18,7} = \psi_{x,y},$$
$$[A]_{18,8} = \psi_{x,x},\ [A]_{18,9} = \psi_{y,y},\ [A]_{18,10} = \psi_{y,x},\ [A]_{19,7} = 3\theta_x,\ [A]_{19,9} = 3\theta_y,$$
$$[A]_{19,11} = 2\psi_x,\ [A]_{19,13} = 2\psi_y,\ [A]_{19,15} = \varphi_x,\ [A]_{19,17} = \varphi_y,$$
$$[A]_{20,8} = 3\theta_x,\ [A]_{20,10} = 3\theta_y,\ [A]_{20,12} = 2\psi_x,\ [A]_{20,14} = 2\psi_y,$$
$$[A]_{20,16} = \varphi_x,\ [A]_{20,18} = \varphi_y,\ [A]_{21,7} = \theta_{x,x},\ [A]_{21,9} = \theta_{y,x},$$
$$[A]_{21,11} = 1/2\psi_{x,x},\ [A]_{21,13} = 1/2\psi_{y,x},\ [A]_{22,8} = \theta_{x,y},\ [A]_{22,10} = \theta_{y,y},$$
$$[A]_{22,12} = 1/2\psi_{x,y},\ [A]_{22,14} = 1/2\psi_{y,y},\ [A]_{23,7} = \theta_{x,y},\ [A]_{23,8} = \theta_{x,x},$$
$$[A]_{23,9} = \theta_{y,y},\ [A]_{23,10} = \theta_{y,x},\ [A]_{23,11} = \psi_{x,y},\ [A]_{23,13} = \psi_{y,y},$$
$$[A]_{24,11} = 3\theta_x,\ [A]_{24,13} = 3\theta_y,\ [A]_{24,15} = 2\psi_x,\ [A]_{24,17} = 2\psi_y,$$
$$[A]_{25,12} = 3\theta_x,\ [A]_{25,14} = 3\theta_y,\ [A]_{25,16} = 2\psi_x,\ [A]_{25,18} = 2\psi_y,$$
$$[A]_{26,11} = \theta_{x,x},\ [A]_{26,13} = \theta_{y,x},\ [A]_{27,12} = \theta_{x,y},\ [A]27,14 = \theta_{y,y},$$
$$[A]_{28,11} = \theta_{x,y},\ [A]_{28,12} = \theta_{x,x},\ [A]_{28,13} = \theta_{y,y},\ [A]_{28,14} = \theta_{y,x},$$
$$[A]_{29,15} = 3\theta_x,\ [A]_{29,17} = 3\theta_y,\ [A]_{30,16} = 3\theta_x^*,\ [A]_{30,18} = 3\theta_y,$$
$$[A]_{31,15} = 1/2\theta_{x,x},\ [A]_{31,17} = 1/2\theta_{y,x},\ [A]_{32,16} = 1/2\theta_{x,y},$$
$$[A]_{32,18} = 1/2\theta_{y,y},\ [A]_{33,15} = \theta_{x,y},\ [A]_{33,17} = \theta_{y,y} \quad (A.5)$$

Individual terms of matrix $[G]$

$$[G]_{1,1} = \partial/\partial x,\ [G]_{2,1} = \partial/\partial y,\ [G]_{3,2} = \partial/\partial x,\ [G]_{4,2} = \partial/\partial y,$$
$$[G]_{5,3} = \partial/\partial x,\ [G]_{6,3} = \partial/\partial y,\ [G]_{7,4} = \partial/\partial x,\ [G]_{8,4} = \partial/\partial y,$$
$$[G]_{9,5} = \partial/\partial x,\ [G]_{10,5} = \partial/\partial y,\ [G]_{11,6} = \partial/\partial x,\ [G]_{12,6} = \partial/\partial y,$$
$$[G]_{13,7} = \partial/\partial x,\ [G]_{14,7} = \partial/\partial y,\ [G]_{15,8} = \partial/\partial x,\ [G]_{16,8} = \partial/\partial y,$$
$$[G]_{17,9} = \partial/\partial x,\ [G]_{18,9} = \partial/\partial y,\ [G]_{19,4} = 1,\ [G]_{20,5} = 1,\ [G]_{21,6} = 1,$$
$$[G]_{22,7} = 1,\ [G]_{23,8} = 1,\ [G]_{24,9} = 1. \quad (A.6)$$

References

[1] Iijima S. Helical microtubules of graphitic carbon. Nature 1991;354:56–8.
[2] Volder MFLD, Tawfick SH, Baughman RH, Hart AJ. Carbon nanotubes: present and future commercial applications. Science 2013;339:535–9.
[3] Griebel M, Hamaekers J. Molecular dynamics simulations of the elastic moduli of polymer-carbon nanotube composites. Comput Methods Appl Mech Eng 2004;193:1773–88.
[4] Song YS, Youn JR. Modeling of effective elastic properties for polymer based carbon nanotube composites. Polymer 2006;47:1741–8.
[5] Han Y, Elliott J. Molecular dynamics simulations of the elastic properties of polymer/carbon nanotube composites. Comput Mater Sci 2007;39:315–23.
[6] Moradi-Dastjerdi R, Foroutan M, Pourasghar A. Dynamic analysis of functionally graded nanocomposite cylinders reinforced by carbon nanotube by a mesh-free method. Mater Des 2013;44:256–66.
[7] Gardea F, Lagoudas DC. Characterization of electrical and thermal properties of carbon nanotube/epoxy composites. Compos B Eng 2014;56:611–20.
[8] Liu Y, Chen X. Evaluations of the effective material properties of carbon nanotube-based composites using a nanoscale representative volume element. Mech Mater 2003;35:69–81.
[9] Chen XL, Liu YJ. Square representative volume elements for evaluating the effective material properties of carbon nanotube-based composites. Comput Mater Sci 2004;29:1–11.
[10] Alibeigloo A. Static analysis of functionally graded carbon nanotube-reinforced composite plate embedded in piezoelectric layers by using theory of elasticity. Compos Struct 2013;95:612–22.
[11] Lin F, Xiang Y. Vibration of carbon nanotube reinforced composite beams based on the first and third order beam theories. Appl Math Model 2014;38:3741–54.
[12] Kamarian S, Pourasghar A, Yas MH. Eshelby–Mori–Tanaka approach for vibrational behavior of functionally graded carbon nanotube-reinforced plate resting on elastic foundation. J Mech Sci Technol 2013;27:3395–401.
[13] Aragh BS, Barati AHN, Hedayati H. Composites: Part B Eshelby–Mori–Tanaka approach for vibrational behavior of continuously graded carbon nanotube-reinforced cylindrical panels. Compos B 2012;43:1943–54.
[14] Ke LL, Yang J, Kitipornchai S. Dynamic stability of functionally graded carbon nanotube-reinforced composite beams. Mech Adv Mater Struct 2012;20:28–37.

[15] Lei ZX, Liew KM, Yu JL. Free vibration analysis of functionally graded carbon nanotube-reinforced composite plates using the element-free kp-Ritz method in thermal environment. Compos Struct 2013;106:128–38.
[16] Janghorban M, Zare A. Free vibration analysis of functionally graded carbon nanotubes with variable thickness by differential quadrature method. Physica E 2011;43:1602–4.
[17] Rokni H, Milani AS, Seethaler RJ. Size-dependent vibration behavior of functionally graded CNT-reinforced polymer microcantilevers: modeling and optimization. Eur J Mech A Solids 2015;49:26–34.
[18] Murmu T, Pradhan SC. Buckling analysis of a single-walled carbon nanotube embedded in an elastic medium based on nonlocal elasticity and Timoshenko beam theory and using DQM. Physica E 2009;41:1232–9.
[19] Formica G, Lacarbonara W, Alessi R. Vibrations of carbon nanotube-reinforced composites. J Sound Vib 2010;329:1875–89.
[20] Shen HS, Zhang CL. Thermal buckling and postbuckling behavior of functionally graded carbon nanotube-reinforced composite plates. Mater Des 2010;31:3403–11.
[21] Shen HS, Xiang Y. Nonlinear analysis of nanotube-reinforced composite beams resting on elastic foundations in thermal environments. Eng Struct 2013;56:698–708.
[22] Shiau LC, Kuo SY. Thermal buckling of composite sandwich plates. Mech Based Des Struct Mach 2004;32:57–72.
[23] Zhu P, Lei ZX, Liew KM. Static and free vibration analyses of carbon nanotube-reinforced composite plates using finite element method with first order shear deformation plate theory. Compos Struct 2012;94:1450–60.
[24] Shen HS. Thermal buckling and postbuckling behavior of functionally graded carbon nanotube-reinforced composite cylindrical shells. Compos B Eng 2012;43:1030–8.
[25] Lin F, Xiang Y. Numerical analysis on nonlinear free vibration of carbon nanotube reinforced composite beams. Int J Struct Stab Dyn 2014;14:1350056.
[26] Yas MH, Samadi N. Free vibrations and buckling analysis of carbon nanotube-reinforced composite Timoshenko beams on elastic foundation. Int J Press Vessels Pip 2012;98:119–28.
[27] Mehrabadi SJ, Aragh BS, Khoshkhahesh V, Taherpour A. Mechanical buckling of nanocomposite rectangular plate reinforced by aligned and straight single-walled carbon nanotubes. Compos B Eng 2012;43:2031–40.
[28] Kerur SB, Ghosh A. Active control of geometrically non-linear transient response of smart laminated composite plate integrated with AFC actuator and PVDF sensor. J Intell Mater Syst Struct 2011;22:1149–60.
[29] Lei ZX, Yu JL, Liew KM. Free vibration analysis of functionally graded carbon nanotube-reinforced composite cylindrical panels. Int J Mater Sci Eng 2013;1:36–40.
[30] Alibeigloo A, Liew KM. Thermoelastic analysis of functionally graded carbon nanotube-reinforced composite plate using theory of elasticity. Compos Struct 2013;106:873–81.
[31] Mohammadi Y, Khalili SMR, Fard KM. Low velocity impact analysis of sandwich plates with functionally graded face sheets. Mech Adv Mater Struct 2016;23:363–74.
[32] Szekrenyes A. Application of Reddy's third-order theory to delaminated orthotropic composite plates. Eur J Mech A Solids 2014;43:9–24.
[33] Wattanasakulpong N, Prusty GB, Kelly DW. Free and forced vibration analysis using improved third-order shear deformation theory for functionally graded plates under high temperature loading. J Sandwich Struct Mater 2013;15:583–606.
[34] Ferreira AJM, Batra RC, Roque CMC. Natural frequencies of functionally graded plates by a meshless method. Compos Struct 2006;75:593–600.
[35] Shen HS, Xiang Y. Nonlinear bending of nanotube-reinforced composite cylindrical panels resting on elastic foundations in thermal environments. Eng Struct 2014;80:163–72.
[36] Lei ZX, Liew KM, Yu JL. Buckling analysis of functionally graded carbon nanotube-reinforced composite plates using the element-free kp-Ritz method. Compos Struct 2013;98:160–8.
[37] Ayatollahi MR, Shadlou S, Shokrieh MM. Multiscale modeling for mechanical properties of carbon nanotube reinforced nanocomposites subjected to different types of loading. Compos Struct 2011;93:2250–9.
[38] S.K. Panigrahi and Y.X. Zhang, Nonlinear finite element analyses of tee joints of laminated composites. In: IOP conference series: materials science and engineering 10:012097. <http://doi.org/10.1088/1757-899X/10/1/012097>; 2010.
[39] Shi H, Salim H, Shi Y, Wei F. Geometric and material nonlinear static and dynamic analysis of space truss structures. Mech Based Des Struct Mach 2015;43:38–56.
[40] Lei ZX, Zhang LW, Liew KM. Free vibration analysis of laminated FG-CNT reinforced composite rectangular plates using the kp-Ritz method. Compos Struct 2015;127:245–59.
[41] Brischetto S. A continuum elastic three-dimensional model for natural frequencies of single-walled carbon nanotubes. Compos B 2014;61:222–8.
[42] Tornabene F, Fantuzzi N, Bacciocchi M, Viola E. Effect of agglomeration on the natural frequencies of functionally graded carbon nanotube-reinforced laminated composite doubly curved shells. Compos B 2016;89:187–218.
[43] Liew KM, Lei ZX, Zhang LW. Mechanical analysis of functionally graded carbon nanotube reinforced composites: a review. Compos Struct 2015;120:90–7.
[44] Brischetto S, Tornabene F, Fantuzzi N, Bacciocchi M. Refined 2D and exact 3D shell models for the free vibration analysis of single- and double-walled carbon nanotubes. Technologies 2015;3:259–84.
[45] Cinefra M, Carrera E, Brischetto S. Refined shell models for the vibration analysis of multiwalled carbon nanotubes. Mech Adv Mater Struct 2011;18:476–83.
[46] Reddy JN. An introduction to nonlinear finite element analysis. Cambridge, UK: Oxford University Press; 2004.
[47] Reddy JN. Mechanics of laminated composite plates and shells: theory and analysis. 2nd ed. Boca Raton, FL: CRC Press; 2004.
[48] Wang ZX, Shen HS. Nonlinear vibration of nanotube-reinforced composite plates in thermal environments. Comput Mater Sci 2011;50:2319–30.
[49] Cook RD, Malkus DS, Plesha ME, Witt RJ. Concepts and applications of finite element analysis. Singapore: John Wiley Sons Pvt. Ltd; 2009.